Astron. Astrophys. 318, 383–389 (1997)

ASTRONOMY
AND
ASTROPHYSICS

ROSAT-HRI observations of the jet in M 87

M. Neumann[1], **K. Meisenheimer**[1], **H.-J. Röser**[1], **and H.H. Fink**[2]

[1] Max Planck-Institut für Astronomie, Königstuhl 17, D-69117 Heidelberg, Germany
[2] Max Planck Institut für Extraterrestrische Physik, Giessenbachstraße 1, D-85740 Garching, Germany

Received 28 May 1996 / Accepted 22 July 1996

Abstract. We present ROSAT-HRI observations of the central region of M 87. By comparison with radio and optical data we investigate whether the X-ray emission of the jet can be explained by the high frequency tail of the radio to optical synchrotron spectrum. We indeed find that knot D and the optically brightest knot A are likely to emit synchrotron X-rays. Although the synchrotron model of the X-ray emission is compatible with the observations at all wavelengths a thermal origin of the X-rays cannot completely ruled out.

Key words: galaxies: M 87; jets – X-ray: galaxies

1. Introduction

Among the large number of extragalactic jets which are conspicuous only by their radio emission, the jet of M 87 plays a key role for a detailed understanding of jet physics. This is mainly due to the fact that the jet can be observed at all accessible wavelengths at high spatial resolution. In particular, studies of its X-ray emission may offer insights into the high energetic processes occurring in extragalactic jets. The synchrotron nature of the radio to optical continuum implies that highly energetic particles ($\gamma \gtrsim 10^6$) must be present throughout the jet (Felten 1968, Stocke et al. 1981, Perez-Fournon et al. 1987, Meisenheimer et al. 1996). Particles of similar high energies are present even in the associated radio lobe (Neumann et al. 1995).

Although the synchrotron model was successful in explaining the radio to optical continuum the origin of the X-ray emission remained an enigma. After Byram et al. (1966) first detected X-ray emission from M 87 Schreier et al. (1982) used the EINSTEIN observatory to re-observe the source at higher resolution. Their map of the central region revealed a double peak structure with one maximum situated at the nucleus and a further one in the jet.

Biretta et al. (1991) reanalyzed the data by subtracting the point-spread function of the EINSTEIN-HRI from the intensity maxima and estimated the X-ray fluxes of knots D, A and B. They found some support for synchrotron X-rays, but the radiation mechanism could not entirely be clarified. By comparison of new X-ray data observed with the more sensitive ROSAT-HRI with the radio to optical synchrotron jet we focus on the question whether the X-ray emission is of synchrotron origin.

Send offprint requests to: K. Meisenheimer

2. ROSAT observation and data reduction

Our observation with the ROSAT-HRI was achieved on June 7$^{\text{th}}$, 1992 during a total integration time of 14239 sec. Using the EXSAS standard reduction package within MIDAS the data have been binned into an image with a pixel scale of $1''/pixel$.

2.1. Point-spread function

Usually, the satellite performs a wobble motion across the source during pointed observations. The standard analysis corrects the raw data for this spacecraft wobble by assigning the single photon events to their respective sky coordinates. This is referred to as aspect solution. The corresponding *aspect error* is on the order of $\sigma_{aspect} = 1''$. We have been trying to correct the data for σ_{aspect} by a re-centering method similar to that described by Röser et al. (1996): First, we divided the total integration time into time bins of 100 sec duration each. From the count events observed during each of these intervals a new image has been created. On the individual images the coordinates of first moment of the intensity distribution have been measured. The difference between the coordinates of a given image and those obtained for the first 100 sec bin yields the positional correction to be applied to all events of the image. After correcting the event coordinates of all bins in this way a new final image has been created. This image in comparison with the original non-recentered map appears washed out, indicating that the angular resolution had been degraded by the process. We therefore conclude that the relatively low ROSAT count-rate of the object (on average 1 cts/sec in a $100'' \times 100''$ field of view) is insufficient to correct for the aspect error. Therefore, we confine all following discussions of our data to the original ROSAT map (Sect. 3.1).

Since the central region of M 87 lacks other point-like ROSAT sources the angular resolution of the data has been estimated from the azimuthally averaged profile of the nucleus.

Table 1.

r [arcsec]	P.A. [degrees]
$1 \leq r \leq 30$	$0 \leq$ P.A. ≤ 90
	$90 <$ P.A. ≤ 180
	$180 <$ P.A. ≤ 220
	$220 <$ P.A. ≤ 360

The resulting value of FWHM = $6\farcs5$ is higher than that of FWHM $\lesssim 5''$ expected from the *ROSAT Users Handbook*. However, due to the unknown influence of the aspect error it is not clear whether this can be attributed to a spatially resolved nucleus.

2.2. Background subtraction for the jet

Two components form the background underneath the jet: a contribution from the nucleus and an extended emission which is the dominating part beyond a distance of $r \simeq 9''$ from the nucleus.

Generally, an extended component is expected even if a point-like source is observed. This is due to the broader wings of the ROSAT PSF. The diffuse extended background surrounding the nucleus and the X-ray knot of M 87, however, cannot be ascribed to this PSF component: the background is highly unsymmetric with respect to both objects or any point between them. Moreover, it is not smoothly distributed and its intensity is higher than that expected from observed PSF's displayed in the *ROSAT Users Handbook* by an order of magnitude. Therefore, we consider the extended emission as an intrinsic background component which has to be modelled and subtracted before the net intensities of the jet and the nucleus can be measured.

To model the background underneath the jet, we considered the azimuthal variation of the intensity within a circle of $30''$ radius centered on the nucleus. This circular area has been divided into several sectors. For the background fit each sector consists of a number of arcs at different distances from the nucleus. Along each arc the intensity is fitted by a polynomal. After these azimuthal fits were achieved, the *coefficients* of the polynomals are fitted into the radial direction in order to smooth the model. The "X-ray knot" which is an unresolved component northwest of the nucleus was excluded from the fit by a mask frame. The mask has been chosen interactively on the screen and its shape was chosen to match the knot.

The following table lists the sectors where background fits were performed. The position angle $P.A.$ is defined counterclockwise from the north (0^o). r is the distance from the nucleus.

Fig. 1 shows the profile of the resulting background model along a line connecting the intensity maximum of the nucleus with that of the X-ray knot. After subtraction of this model from the original map, the background corrected count-rate of the knot has been measured on the image shown in Fig. 2a.

Fig. 1 also shows a striking asymmetry of the nucleus which indicates an additional emission component. In the case of synchrotron X-rays discussed in Sect. 5.1, it can be attributed to the innermost part of the optical jet (knot D, $r = 3''$ from the core).

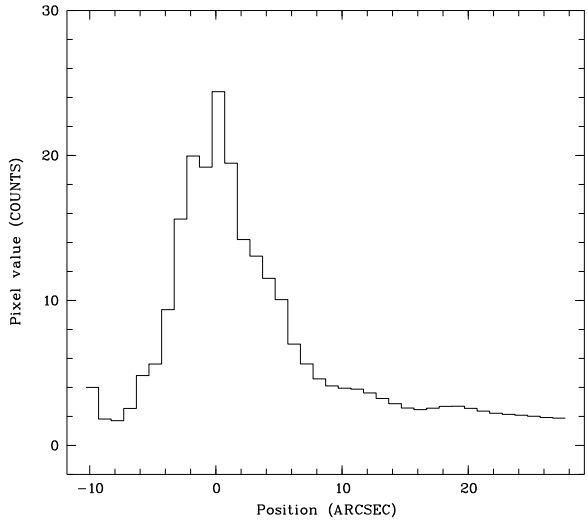

Fig. 1. Run of the modelled background along a line connecting the nucleus with the jet.

Table 2.

r [arcsec]	P.A. [degrees]
$5 \leq r \leq 30$	$0 \leq$ P.A. ≤ 60
	$60 <$ P.A. ≤ 180
	$180 <$ P.A. ≤ 270
	$270 <$ P.A. ≤ 360

2.3. Background subtraction of the nucleus

For the background subtraction of the nucleus the same computational method as for the X-ray knot has been used. The center of the fitted circular area, however, was now moved to the maximum of the knot.

It was assumed that the X-ray knot, whose emission is visible up to $r = 5''$ from its maximum, does not contribute to the background level at the position of the nucleus. Thus, the model only fits isophotes beyond $r = 5''$ from the maximum of the knot. Similar to the fit method described in the previous section, the nucleus was excluded from the fit by an interactively chosen mask. The resulting background model to be subtracted from the original map then contains the background model at $r > 5''$ from the knot and the *original* pixelvalues of the knot at $r < 5''$. What remains after subtraction of the model frame is the background corrected nuleus, but the pixel values within $r = 5''$ from the knot are zero since the knot itself was subtracted. These zero values correspond to the "hole" in the centre of Fig. 2b).

The following table specifies the fitted area and its division into sectors.

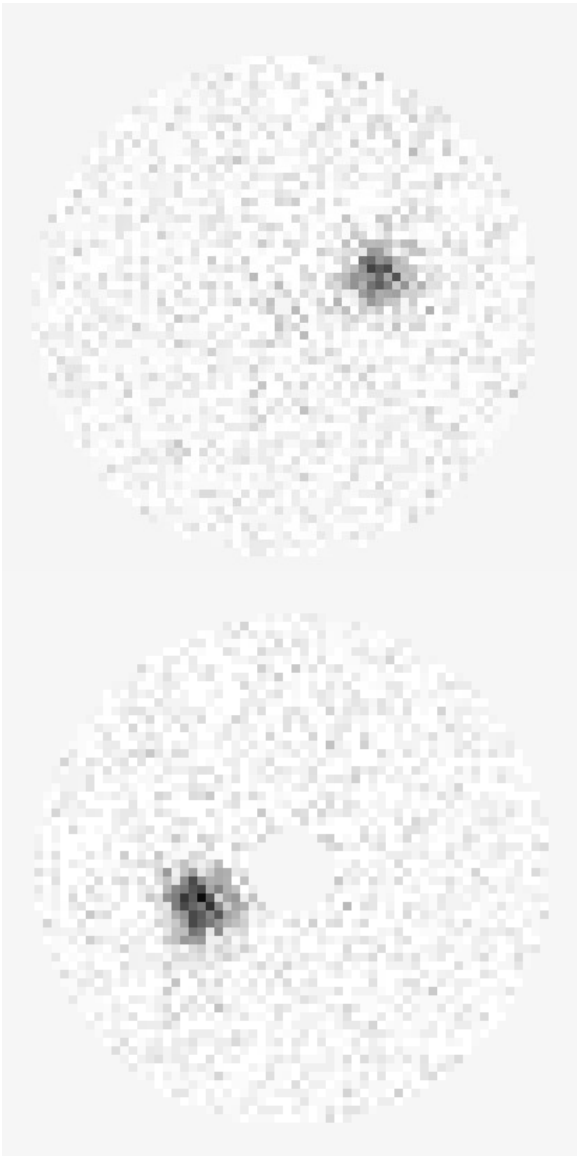

Fig. 2. a Top: Jet of M 87 after subtraction of the nucleus and the extended background emission. **b** Bottom: Nucleus after background subtraction. Note, that the center of each image is the chosen center of the respective azimuthal fit. Thus, the center of Fig. 2a is the position of the nucleus while Fig. 2b is centered on the X-ray knot.

2.4. Count to flux conversion

First, the counts derived from the ROSAT map have been divided by the dead time corrected integration time of 13.995 ksec which is 1.7 % lower than the total integration time given above.

Generally, an observed count-rate depends on the X-ray spectrum of the source, the galactic absorption and on the spectral response function of the detector. The X-ray flux density corresponding to the measured count-rate of the jet was obtained by synthetic photometry: first, for an assumed unabsorbed photon spectrum $C_\nu = S_{\nu,\mathrm{o}} \times (\nu/\nu_x)^\alpha / h\,\nu$ the expected ROSAT count-rate has been calculated. $\nu_x = 2.8 \times 10^{17}$ Hz is the center frequency of the ROSAT band. $S_{\nu,\mathrm{o}}$ is an *assumed* flux density

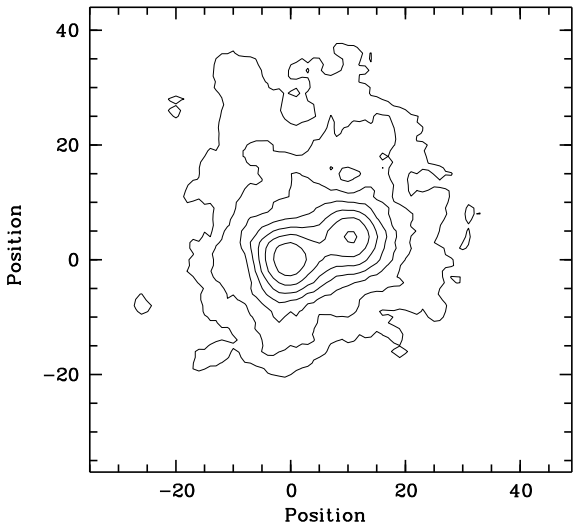

Fig. 3. ROSAT-HRI image of the central region of M 87. The map has been smoothed with an FWHM = 3″ beam resulting in an effective resolution of FWHM = 7.″2. The lowest contour level is 0.116 cts/ksec/pixel and the ratio of adjacent contour levels is $\sqrt{2}$. The axes plot distances relative to the nucleus in arcsec.

at $\nu = \nu_x$. Using the column density of $N_{HI} = 2.4 \times 10^{20}$ cm^{-2} (Biretta et al. 1991) this spectrum has been corrected for galactic absorption. By a subsequent convolution of this spectrum with the energy dependent effective area $\sigma\,(E)$ of the combination of ROSAT-HRI and X-ray mirror as given by the *ROSAT Users Handbook* the expected ROSAT count-rate C_{exp} has been calculated. The result has been compared with the measured count-rate C_{obs} which yields the desired flux density $S_{\nu\,\mathrm{obs}}$: $S_{\nu\,\mathrm{obs}} = S_{\nu,\mathrm{o}} \times C_{\mathrm{obs}}/C_{\mathrm{exp}}$.

3. Results

3.1. X-ray map

Fig. 3 shows our map of the central region of M 87 observed with the ROSAT-HRI on June 7^{th} 1992. Two distinct peaks are clearly visible. Both components are embedded into a weak diffuse background emission. Following the suggestion of Schreier et al. (1982) we assign the eastern maximum (left) to the nucleus. In the following sections the northwesterly maximum (X-ray knot) is regarded as an emission from the jet.

3.2. Intensity measurements

After subtracting the background models described in Sects. 2.2. and 2.3. the counts of the nucleus and of the X-ray knot have been measured within circular apertures of 6″ radius centered on the intensity maxima of these components. The X-ray knot then yields 532 cts corresponding to a count-rate of 0.038 cts/sec. The respective values for the nucleus are 839 cts and 0.060 cts/sec.

We now ask for the flux density of the X-ray knot corresponding to the background corrected count-rate. The flux density obtained from the procedure described in Sect. 2.4 depends

on the assumed X-ray spectrum. First, we assume that the X-ray knot is due to the high frequency synchrotron tail of the region A+B+C which forms the brightest part of the optical jet. In this case its radio to optical spectrum must continue smoothly into the ROSAT band. This would result in a spectral index of $\alpha_{ox} = -1.45$ (cf. Meisenheimer et al. 1996) and in a flux density of $S_\nu = 159$ nJy. Another non-thermal mechanism, the inverse Compton scattering of low energetic photons by the relativistic particles emitting the radio to optical synchrotron spectrum ($\alpha_{ro} = -0.66$), yields $S_\nu = 251$ nJy. Assuming instead an optically thin plasma emitting thermal bremsstrahlung ($\alpha = -0.1$) we obtain $S_\nu = 317$ nJy. In Sect. 5 we discuss these radiation mechanisms in detail. The combined error of the flux densities which results from background subtraction and placement of the aperture is estimated to be 6%.

4. Comparison with EINSTEIN data

Comparing the map of Fig. 3 with the 44.66 ksec EINSTEIN image of Biretta et al. (1991) which has a comparable signal-to-noise ratio we find a nearly perfect agreement of the observed morphologies.

X-ray count rates and flux densities of the jet have so far been derived by three groups. The third column of Table 3 lists our background subtracted flux for $\alpha = -1.3$ together with their results. Since all observations refer to different center frequencies $< \nu >$ the fifth column shows the EINSTEIN fluxes transformed to the center frequency of the ROSAT band.

The listed ROSAT count-rate refers to the $10'' \times 10''$ box also used by Schreier et al. (1982). This in turn corresponds to the sum about knots A+B of the fluxes given by Biretta et al. (1991).

Harris et al. (1996) compared their new ROSAT-HRI observations with our data and the EINSTEIN data and pointed out to us a possible variability of the jet flux. Table 3 compares our jet flux with that observed with EINSTEIN. This takes into account the different center frequencies $< \nu >$ of the ROSAT and EINSTEIN bands: extrapolating the EINSTEIN fluxes into the ROSAT band we find flux densities $\simeq 1.6$ times higher than our result. The discrepancy is nearly independent of the assumed spectral index. We find a difference of $\simeq 6\,\sigma$ if errors of $\sim 6\,\%$ are assumed for all flux densities.

5. Discussion of radiation mechanisms

Using our ROSAT map and the background subtracted X-ray fluxes of the jet given in Sect. 3.2 together with radio and optical observations (cf. Meisenheimer et al. 1996) we now discuss different scenarios of the physical origin of the X-ray emission.

5.1. Synchrotron radiation

A first test of the synchrotron model consists of a comparison of the X-ray morphology with data of the synchrotron jet observed at lower frequencies. Synchrotron X-rays are preferentially expected at those knots of the jet where the locally observed optical synchrotron spectrum is the flattest. Meisenheimer et al. (1996) find the flattest optical spectra in knots D ($r = 3''$) and A ($r = 12\farcs7$) where spectral indices of $\alpha_{opt} \simeq -0.8$ are observed. All other knots exhibit steeper optical spectra with α_{opt} reaching from -0.95 at knot F to -1.15 at knot G.

Due to the close proximity of knot D to the nucleus synchrotron X-rays from the knot would not be resolved in the ROSAT map. Figs. 1 and 3 indicate, however, an emission component which contributes to the maximum of the nucleus and which can be traced out to a distance of at least $r \simeq 5''$. This additional component is consistent with the run of α_{opt}. Thus, knot D is indeed likely to contribute to the X-ray emission of the jet.

According to the run of α_{opt} the X-ray maximum of the jet (i.e. the "X-ray knot"), if caused by the synchrotron mechanism, is most likely to originate from knot A. Thus, its distance r_x from the nucleus measured on the ROSAT map must be consistent with the position of the optical knot. Since we now assume pure synchrotron radiation, we have to bear in mind that r_x as measured on the ROSAT map may be influenced by the contribution of knot D to the maximum of the nucleus. The unresolved emission from knot D effectively shifts the measured position of the nucleus to the northwest and thus shortens the measured distance r_x by $0\farcs3$. After correcting for this contribution the intensity maximum of the X-ray knot is found at $r_x = 11\farcs9 \pm 0\farcs2$ from the core. In order to test if this result is consistent with synchrotron X-rays from knot A we compared the background corrected intensity profile of the X-ray knot with that of the optical synchrotron jet (Fig. 4). For this purpose the ROSAT image and an optical R band map have been convolved to a common beam. The convolved jet profiles were obtained by a weighted summation (cf. Röser and Meisenheimer 1991) of the counts within elliptical apertures positioned along the jet axis. The major axis of each aperture was aligned perpendicular to the jet axis. In this way, the summation not only includes the peak intensities measured along the jet axis but also contains the counts observed aside the axis. This enhances the signal-to-noise-ratio of the resulting X-ray profile considerably. The weighting function is a gaussian with half widths $\mathrm{FWHM}_{\mathrm{w,\,x}}$, $\mathrm{FWHM}_{\mathrm{w,\,y}}$ where x and y corresponds to the coordinate along and perpendicular to the jet axis, respectively. The summation then corresponds to a convolution with a beamwidth of the convolved image of

$$\mathrm{FWHM}_{\mathrm{i,\,eff}} = \sqrt{\mathrm{FWHM}_{\mathrm{o}}^2 + \mathrm{FWHM}_{\mathrm{i,\,w}}^2} \qquad \mathrm{i} = \mathrm{x},\ \mathrm{y}$$

$\mathrm{FWHM}_{\mathrm{o}}$ is the point-spread function of the map. $\mathrm{FWHM}_{\mathrm{i,\,eff}}$ is the beam width after the convolution. The common elliptical beam of the convolved X-ray and optical maps is then $\mathrm{FWHM}_{\mathrm{x,\,eff}} \times \mathrm{FWHM}_{\mathrm{y,\,eff}} = 5\farcs5 \times 9\farcs4$. The convolution of the ROSAT map is based on an angular resolution of $\mathrm{FWHM}_{\mathrm{o}} = 5''$ taken over from the ROSAT Users Handbook since our data do not allow to derive a reliable point-spread function.

Fig. 4 shows that the intensity maximum of the convolved X-ray profile is found more than $1''$ away from the optical maximum at $r = 13\farcs4$. Synchrotron X-rays must therefore be emitted

Table 3. Comparison between ROSAT and EINSTEIN observations of the jet. [1]: this work, [2]: Schreier et al. (1982), [3]: Biretta et al. (1991)

Telescope	$< \nu >$ [Hz]	C_{jet} [cts/sec]	$S_\nu^{(\alpha=-1.3)}$ $(< \nu >)$ [nJy]	$S_\nu^{(\alpha=-1.3)}$ $(2.8 \times 10^{17}\,\mathrm{Hz})$ [nJy]	Reference
ROSAT-HRI	2.8×10^{17}	0.042	200	200	[1]
EINSTEIN-HRI	4.0×10^{17}	0.033	200	318	[2]
		0.036	219	348	[3]

mainly around $r_x = 12''$ whereas the knots situated beyond this location (knots B, C and G) do not contribute significantly.

The comparison of the X-ray profile with the 2 cm radio intensity (Owen et al. 1989, bottom panel of Fig. 4, FWHM = $0\farcs1$) reveals that the X-ray maximum is situated $0\farcs4$ nearer to the nucleus than the radio maximum of knot A ($r = 12\farcs3$). We therefore conclude that synchrotron X-rays are not emitted at the position of the radio maximum. They are rather emitted at a position between knot I and the maximum of knot A where the intensity rises steeply. In the remainder of the section this location is referred to as the "front-side" of knot A.

We thus consider the possible radio to X-ray spectrum of the front-side. The brightest part of the radio to optical jet consists of knots A, B and C which contribute about 83% of the total jet flux. Fig. 5 shows the spectrum of this region as a solid line. Between radio and optical wavelengths the spectrum is dominated by a power law with a spectral index of $\alpha = -0.66$ that cuts off steeply beyond the optical.

Knot A dominates the emission of the region A+B+C. Therefore, we now assume the spectrum of the front-side to have the same spectral shape as the whole region whose spectrum is shown as a solid line (Meisenheimer et al. 1996) in Fig. 5. In our simple approach we scaled down this spectrum to get the spectrum of the front-side. We obtained the scaling factor by comparison of the 2 cm flux density S_{ABC} with that of the front-side. The flux density of the front-side has been derived from its intensity profile perpendicular to the jet as given by Owen et al. (1989). They divide the radio jet into several slices perpendicular to the jet axis, each with a thickness of $0\farcs25$. The front-side corresponds to component A 1 in their nomenclature. Its intensity profile has been integrated over the spatial extend perpendicular to the jet axis and multiplied by the slice thickness. This results in a flux density of S_ν (2 cm) = 331 mJy.

In order to find the ROSAT flux density corresponding to the synchrotron spectrum of the front-side we assumed that the down-scaled $\alpha = -0.66$ power law cuts off at some *arbitrary* frequency ν_c. This spectrum was convolved with the combined spectral response function of the X-ray mirror and HRI detector which yielded the expected ROSAT count-rate $C_{\rm exp}$. If $C_{\rm exp}$ was lower than the observed value $C_{\rm obs}$ the spectral cut-off has been shifted to a higher frequency. This was iterated until $C_{\rm exp} = C_{\rm obs}$. The observed count-rate can be reproduced if the power law cuts off steeply in the ROSAT band. At the center frequency of the band the corresponding flux density is $S_x\,(2.8 \times 10^{17}\,\mathrm{Hz}) = 2.5$ nJy. The spectrum connecting this ROSAT flux with the 2 cm flux density is shown as a dashed line in Fig. 5. The inset of Fig. 5 explains the origin of the low X-ray flux density: since the spectrum of the frontside is very steep throughout the ROSAT band ($< \alpha > = -5.8$) the resulting X-ray flux strongly depends on the reference frequency. The center frequency of $< \nu > = 2.8 \times 10^{17}$ Hz derived from the spectral response function ε_ν of the ROSAT band (solid line of the inset) is situated near the maximum value of ε_ν. At this frequency the spectrum has dropped off to very low fluxes. Thus, ε_ν pronounces the lower flux densities of this spectrum. A flux density weighted frequency of 5.4×10^{16} Hz can be obtained from the convolution of ε_ν with the steep spectrum. If this frequency is used instead the flux density amounts to 3.5 μJy ($\triangle$)[1]

The spectrum of the front-side can also be used to calculate the expected EINSTEIN count-rate. The convolution of the spectrum with the EINSTEIN spectral response function yields 0.011 cts/sec which is more than three times lower than the values given by Schreier et al. (1982) and Biretta et al. (1991). Note, that the synchrotron spectrum used for the convolution has been adjusted to the ROSAT count-rate observed 13 yr later. The predicted EINSTEIN countrate is $10\,\sigma$ lower than the observed values. Thus, provided that the X-rays are synchrotron emission, our simple model gives support to the X-ray variability of the jet proposed by Harris et al (1996). The comparison suggests that the X-ray count-rate has decreased since the observation with EINSTEIN.

A variability of synchrotron X-rays may be explained by very slight shifts of the spectral cutoff along the frequency axis: since the spectrum is steep in the ROSAT and EINSTEIN bands a slightly decreasing cut-off frequency would cause the count-rate to decrease significantly. Such variations of ν_c are possible since the particles emitting synchrotron X-rays exhibit high Lorentz factors of $\gamma_c = 1.9 \times 10^7$ if the *minimum energy* estimate of $B_{me} = 64$ nT (cf. Meisenheimer et al. 1996) is assumed for the local magnetic field. At the spectral cutoff, a time of the

[1] The spectrum assumed for the frontside is the scaled synchrotron model spectrum of region A+B+C. It has a steep high frequency cut-off. However, the IR to optical fluxes of A+B+C do not allow to decide between a steep and a smoother cut-off (see Sect. 4.4 of Meisenheimer et al. 1996). A smoother cut-off of the scaled spectrum would yield a higher flux of the front-side at the center frequency of the ROSAT-HRI band. The difference to the X-ray flux at the flux density weighted frequency would then be smaller.

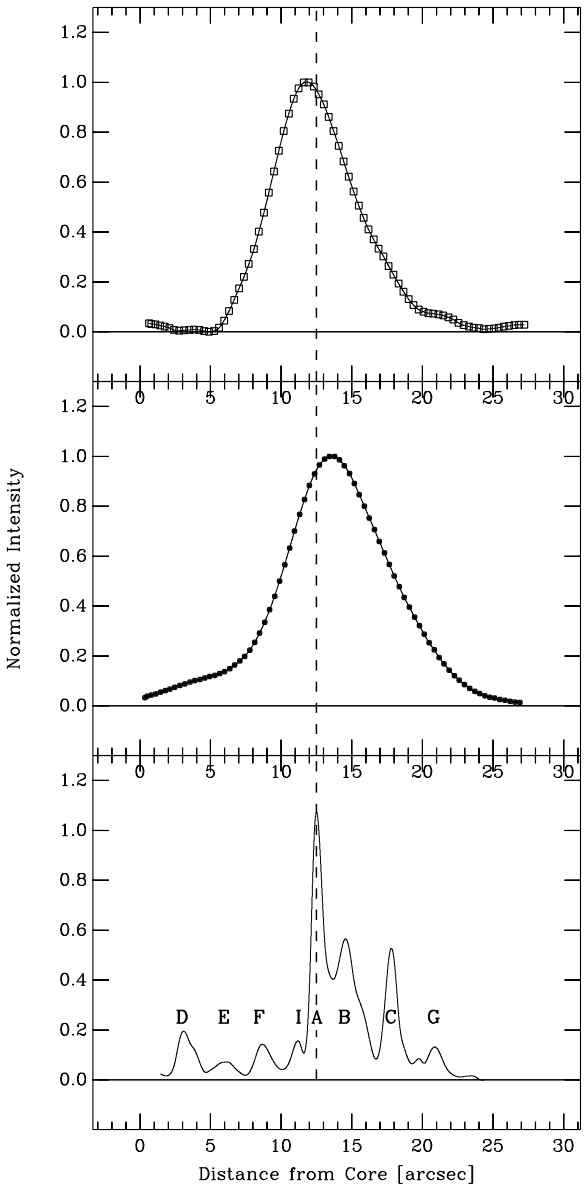

Fig. 4. Comparison of the X-ray profile (top, □) with the optical R band profile (centre, •) at a common angular resolution of FWHM = 5.″5 × 9.″4 with the major axis aligned perpendicular to the jet axis. Bottom: 2 cm radio profile (Owen et al. 1989), FWHM = 1.″3. The dashed line marks the 2 cm position of knot A.

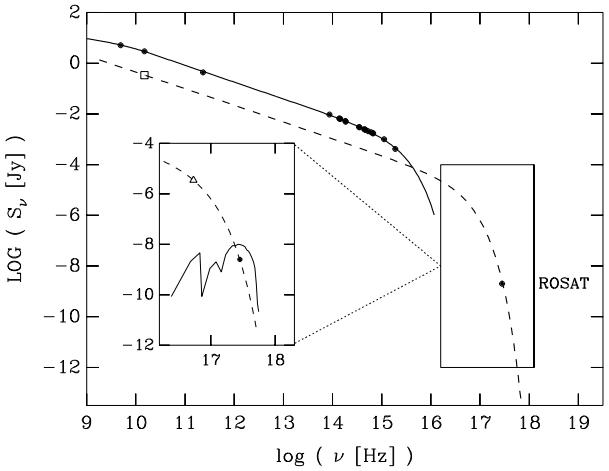

Fig. 5. Possible radio to X-ray spectrum of the front-side of knot A (dashed curve) in comparison to the spectrum of the region of knots A+B+C (solid curve, Meisenheimer et al. 1996). Inset: blow-up of the high frequency tail enclosed by the rectangle. The flux densities at the center frequency of the ROSAT-HRI band (•) and at the flux-weighted frequency (△) are shown. The solid line gives the shape of the combined spectral response functions (ε_ν) of the ROSAT-HRI and the X-ray mirror assembly.

order of the synchrotron lifetime ($\simeq$ 5 yr) is needed to replenish the high radiative losses of the emitting particles.

If the cut-off Lorentz factor γ_c decreases by $\Delta\gamma/\gamma$ = 33% the cut-off frequency decreases by 55%. This spectral shift X-ray diminishes the X-ray count-rate by three times as found above. The emitting particles lose the corresponding amount of energy $\Delta E = \Delta\gamma_c\, m\, c^2$ within 1.5 yr. Therefore, a variation of the X-ray flux during the 13 yr interval between the ROSAT and EINSTEIN observations would not be exceptional. While the X-ray flux changes the IR to optical fluxes would remain unaffected since the corresponding particle lifetimes at these lower frequencies are larger by an order of magnitude. This can be confirmed by a comparison of our recent infrared observations with older optical data: The extrapolation of B, R and I band flux densities observed in 1988 (Meisenheimer et al. 1996) is indeed consistent with our H and K band observations of 1994 (Neumann et al. 1996) for all knots of the jet. Moreover, our IR data are in excellent agreement with the IR fluxes observed 14 yr earlier by Stocke et al. (1981).

The foregoing discussion has shown that all X-ray properties of the jet observed with ROSAT can be well understood by assuming synchrotron radiation in the ROSAT band. However, the ROSAT data cannot exclude other models. In particular, the morphological deviation of the X-ray emission from the optical synchrotron jet might point to another origin. Therefore, alternative scenarios are discussed in the following sections.

5.2. Alternative explanations

5.2.1. Inverse Compton radiation

In the jet of M 87 charged relativistic particles lose their energy by synchrotron radiation. If in addition low energetic photons are present the relativistic particles transfer some energy to the photons by Compton collisions. By this *inverse Compton scattering* the initial photons may reappear as X-rays in the ROSAT band. The input photons can be generated externally or by the synchrotron emitting charges itself (synchrotron self-Compton emission, SSC). In both cases the ratio of the synchrotron power P_{sync} and the inverse Compton scattered power P_{IC} is given by (cf. Longair 1994)

$$\frac{P_{IC}}{P_{sync}} = \frac{u_{rad}}{u_{mag}}$$

where u_{rad} is the energy density of the radiation to be scattered and $u_{mag} = B^2/2\,\mu_o$ ($\mu_o = 4\,\pi \times 10^{-7}$ V sec A^{-1} m^{-1}) is the energy density of the magnetic field B in the jet. For B we used the minimum energy field strength $B = B_{me}$ estimated by Meisenheimer et al. (1996).

P_{IC} has been calculated from the X-ray flux integrated over the width of the ROSAT band. P_{sync} is the frequency integrated synchrotron flux density produced by the scattering particles. Thus, the left-hand side of the equation depends completely on observed quantities. This ratio was compared with the value of the right-hand side which depends on the assumed source of input photons. In our estimations they are supplied by the 2.7 K background, the starlight of the elliptical galaxy of M 87 and by the synchrotron radiation, respectively. It turns out that none of these sources produces a radiation density high enough to satisfy the above condition i.e. to explain the observed X-ray power P_{IC}. In all cases the resulting Compton scattered X-ray flux is at least two orders of magnitude lower than the observed value.

For a highly relativistic jet which is not aligned to the observer the synchrotron radiation is beamed into the direction of motion. In this case the *intrinsic* synchrotron energy density might be high enough to operate the SSC efficiently. For the jet of M 87 such scenarios are unlikely, however, since the proper motions of single knots are rather mildly relativistic ($\beta_{jet} \lesssim 0.5$, Biretta et al. 1995). Moreover, the jet stretches smoothly into the western radio lobe without the presence of a hot-spot where a relativistic flow might be decelerated (cf. Biretta and Meisenheimer 1993).

5.2.2. Thermal bremsstrahlung

In the simplest version of thermal bremsstrahlung the X-rays are produced by an optically thin spherical cloud of gas with a temperature of $T = 3 \times 10^7$ K. Since the X-ray knot of the jet appears unresolved its radius cannot be larger than 200 pc. The measured count-rate is converted into a flux for an assumed spectral index of $\alpha = -0.1$. From the flux, the distance and the volume of the source of $V = 2.6 \times 10^{56}$ m^3 a luminosity of $L_\nu = 1.1 \times 10^{16}$ W/Hz and an emissivity of $\varepsilon_\nu = L_\nu/V = 7.5 \times 10^{-21}$ W m^{-3} Hz^{-1} results. The emissivity implies a particle density of $n = 7.2 \times 10^6$ m^{-3}, a mass of $M = 5.2 \times 10^6\,M_\odot$ and a cooling time of $t_{cool} = 3 \times 10^6$ yr.

Models describing the distribution of the hot gas in the central region of M 87 (cf. Hardee et al.1993) yield number densities and Temperatures in the surroundings of knot A of $n \lesssim 10^6$ m^{-3} and $T \sim 10^8 \ldots 10^9$ K. The resulting gas pressure is $\sim$ 100 times lower than the pressure estimated for the X-ray knot. Thus, a pressure equilibrium is not obtained. This, however, does not exclude thermal X-rays: the intensity maximum of the X-ray jet is observed where the jet – which has a constant opening angle of $6\overset{\circ}{.}5$ between the nucleus and knot A – re-collimates. The X-ray emission may therefore indicate an interaction of the jet with its surroundings. It seems probable that this produces shocks propagating into the ambient gas. The shocks may compress and heat the gas with subsequent cooling by X-ray emission.

6. Conclusions

Our comparisons of the ROSAT-HRI map with the radio/optical synchrotron jet show that the X-ray morphology is consistent with the morphology of the radio/optical synchrotron jet as well as with the behaviour of the radio to optical spectra along the jet axis. We therefore consider the synchrotron model as a reasonable explanation of the X-ray jet. Inverse Compton scattering of low energetic photons supplied by external sources or by the jet itself are unlikely to produce the X-ray emission. On the base of our current data a thermal origin of the X-ray emission cannot completely ruled out.

In order to test the synchrotron model of the X-ray emission further optical and UV data observed with the HST would be useful. From these maps the run of the high frequency spectral index along the jet axis can be derived at an angular resolution of FWHM = $0\overset{''}{.}2$. If our interpretation is correct, we would expect to find a straight power law $S_\nu \propto \nu^{-0.66}$ at the front-side of knot A.

Acknowledgements. We are grateful to Dan Harris, SAO, for communicating to us the results of his variablity analysis prior to publication. We also want to thank F.N. Owen, NRAO, who provided the 2 cm VLA map of M 87 in digital form.

References

Biretta, J.A., Stern, C.P., Harris, D.E., 1991, AJ 101, 1632
Biretta, J.A, Meisenheimer, K. in H.-J. Röser, K. Meisenheimer (eds.): "Jets in Extragalactic Radio Sources", Proceedings of a Workshop held at Ringberg Castle, Springer Berlin Heidelberg 1993, p. 159
Biretta, J.A., Zhou, F., Owen, F.N., 1995, ApJ 447, 582
Byram, E.T., Chubb, T.A., Friedman, H., 1966, Science 152, 66
Hines, D.C., Owen, F.N., Eilek, J.A., 1989, ApJ 347, 713
Hardee, P.E., White, R.E., Norman, M.L. in H.-J. Röser, K. Meisenheimer (eds.): "Jets in Extragalactic Radio Sources", Proceedings of a Conference held at Ringberg Castle, Springer Berlin Heidelberg 1993, p. 193
Harris, D.E., Biretta, J.A., Junor, W., 1996, in prep.
Longair, M.S., High Energy Astrophysics Vol. 2, Cambridge University Press 1994
Meisenheimer, K., Röser, H.-J., Hiltner, P.R., Yates, M.G., Longair, M.S., Chini, R. Perley, R.A., 1989, A&A 219, 63
Meisenheimer, K., Röser, H.-J., Schlötelburg, 1996, A&A, 307, 61
Neumann, M. Meisenheimer, K., Röser, H.-J., Stickel, M., 1995, A&A 292, 662
Neumann, M., PhD Thesis, Universität Heidelberg 1995
Neumann, M., Meisenheimer, K., Röser, H.-J., 1996, A&A in prep.
Owen, F.N., Hardee, P.E., Cornwell, T.J., 1989, ApJ 340, 698
Röser et al., 1996, A&A in prep.
Schreier, E.J., Gorenstein, P., Feigelson, E.D., 1982, ApJ 261, 42
Stocke, J.T., Riecke, G.H., Lebofsky, M.J., 1981, Nature 294, 319

This article was processed by the author using Springer-Verlag LaTeX A&A style file *L-AA* version 3.